ChemPubSoc Europe

DOI: 10.1002/celc.201402372

CHEMELECTROCHEM Articles

Ultrasonic Electrochemical Reaction on Boron-Doped Diamond Electrodes: Reaction Pathway and Mechanism

Hongying Zhao,[a] Guangfeng Wei,[b] Junxia Gao,[a] Zhipan Liu,*[b] and Guohua Zhao*[a]

An ultrasound-enhanced electrochemical oxidation process with boron-doped diamond anodes is adopted and used for removing bisphenol A. The reaction activity and mechanism is evaluated and explained through experimental and theoretical methods. The structure and stability of the anode surface are illustrated and the electrochemical oxidation channels leading to ·OH formation are proposed using density functional calculations. Ultrasound increases the diffusion and mass transfer of ·OH at a high working potential (i.e., 3.0 V), while enhancing the collision frequency between organic pollutants and *O radicals at low working potentials (i.e., 1.7 V). The main intermediates determined by HPLC are hydroquinone, maleic and oxalic acids in both processes, suggesting the same degradation pathway even with ultrasound.

1. Introduction

New advanced oxidation processes based on electrochemical technology, called electrochemical advanced oxidation processes (EC),[1] are well known as a green technology due to its excellent oxidation ability without secondary pollution and has been widely applied in the treatment of biologically persistent organic pollutants. Electrochemical oxidation ability are determined by direct electrolysis and/or indirect electrolysis.[2] That is to say, EC is not only applied to the direct oxidation of pollutants on the anode surface but it also promotes the generation of mediated oxidants which can act the electrode surface and extend the oxidation process to the bulk solution.[3] In the area of EC oxidation, boron-doped diamond (BDD) electrodes exhibit excellent electrochemical properties, including a wide potential window, low double-layer capacitance, chemical inertness, and structural stability.[4] These properties make BDDs a promising material for EC oxidation of refractory pollutants. Moreover, in order to further improve the efficiency of EC oxidation, simultaneous use of other advanced oxidation technologies are exploited. Among these technologies, ultrasound (US) is effective in treating toxic effluents and reducing toxicity. Bisphenol A (BPA), considered as an emerging pollutant, is frequently encountered in waste water and in surface water.[5] Many studies have shown that BPA could cause harmful effects such as abnormal physiological changes, reproductive impairments, and testicular and breast cancer.[6] Thus, in this work BPA was selected as a model target contaminant for assessing the reaction activity.

One of the key points to explain the high efficiencies reached by EC process is the understanding of its role in mediated oxidation processes. The electrochemical properties of BDD electrodes are determined by their surface composition, thus it would be very useful to know the stable structure of the BDD surface through description of its special electrochemical environment at the atomic level. Theoretical modeling based on density functional theory (DFT) calculations[7] has demonstrated its ability to provide a detailed mechanism and kinetics for surface reactions, and has been applied to complex electrocatalytic reactions in the last few years.

In this work, theoretical modeling is utilized to understand the key oxidants during the degradation of BPA during ultrasonic electrochemical oxidation (US–EC). In particular, the reaction channel for the potential-dependent kinetics of hydroxyl radical (·OH) generation is resolved from DFT. Based on the results from experiment and theory, the ·OH generation mechanism on the BDD electrode and the catalytic role of US are systemically discussed. We show that US–EC oxidation on BDD is an efficient electrochemical oxidation system for ·OH generation at high potentials and the enhanced diffusion kinetics facilitated by US.

2. Results and Discussion

A comparative study was performed in this work to investigate the improvement for removing BPA in electrochemical treatment with the aid of US. The removal of BPA (A) and the chemical oxygen demand (COD) (B) versus time is shown in Figure 1. In US–EC system, the fraction of BPA removed by 4 h is 98%, an increase of 24% compared to the EC process (79%). The time needed to reach the same BPA removal in EC process (95%) is 8 h, twice as long as for the US–EC process. That

[a] Dr. H. Zhao,[+] Dr. J. Gao, Prof. Dr. G. Zhao
Department of Chemistry
Tongji University
1239 Siping Road, Shanghai 200092 (China)
E-mail: g.zhao@tongji.edu.cn

[b] Dr. G. Wei,[+] Prof. Dr. Z. Liu
Shanghai Key Laboratory of Molecular Catalysis and Innovative Materials
Department of Chemistry
Key Laboratory of Computational Physical Science
Fudan University
220 Handan Road, Shanghai 200433 (China)
E-mail: zpliu@fudan.edu.cn

[+] These authors contributed equally to this work

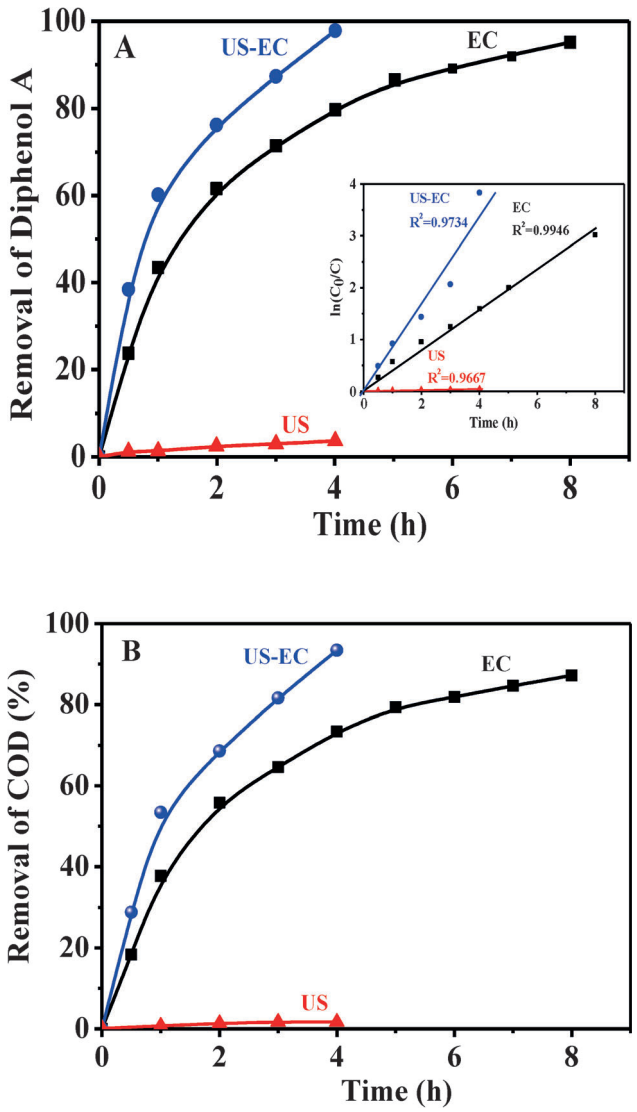

Figure 1. Removal of A) BPA and B) COD with treatment time for a 50 mg L^{-1} BPA solution on the BDD electrode. In the inset the linear plots of $\ln(C_0/C)-t$ for the treatment of 50 mg L^{-1} BPA solution gives the kinetics of BPA as pseudo-first-order.

means that the degradation efficiency can be improved with the aid of US on BDD electrode. Ultrasonic irradiation of aqueous solutions is well known for yielding sonochemistry via cavitation, which can cause physical effects to improve mass transport and chemical effects to activate substrates. However, with ultrasound alone, only 3.7% BPA was degraded, possibly due to the small amount of ·OH generated via cavitation. These results indicate that the enhanced efficiency can most likely be attributed to the improvement afforded by the EC process and the activation of BDD electrode surface, not only owing to the sonochemical effect. The obtained BPA removal data were further analyzed by kinetic modeling. Good linear plots were obtained when fitted to a pseudo first-order reaction (inset of Figure 1 A). The pseudo first-order rate constant (k) in the US–EC process is 2.7×10^{-4} s^{-1}, 2.7 times and 100 times faster respectively than the EC (1.0×10^{-4} s^{-1}) and the US processes (2.6×10^{-6} s^{-1}).

The removal of COD in the reaction solution is determined as an indicator for the organic mineralization at different time intervals and is plotted in Figure 1 B. After 4 h, 94% of COD has been removed in the US–EC process, whereas only 73% of COD has been eliminated in the EC process. The complete mineralization time is 4.5 and 9.3 h in the US–EC and EC processes, respectively. So the time needed to reach mineralization is shortened by 52% with ultrasound irradiation. This further suggests that the US–EC method is efficient for the degradation of BPA.

The generated ·OH radical can be used to efficiently oxidize a wide variety of organics though indirect electrolysis in electrochemical oxidation. To some extent, the amount of generated ·OH can reflect the activity of the electrode and the reaction system.[8] Figure 2 plots the concentration of ·OH ($C_{\cdot OH}$) in the

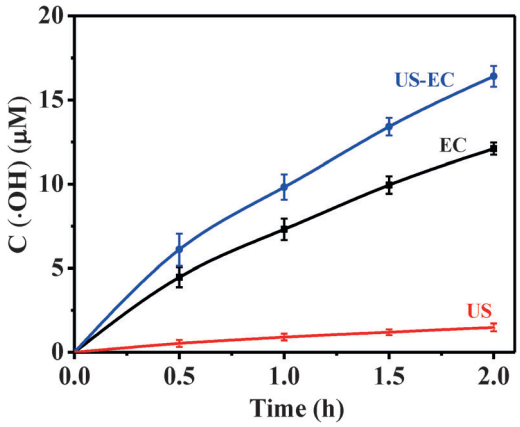

Figure 2. Evolution of the hydroxyl radical during the degradation of a 50 mg L^{-1} BPA solution.

degradation solution. This shows that $C_{\cdot OH}$ increases with increasing treatment time. The $C_{\cdot OH}$ in the US–EC process increases to 16.0 μM at 2 h—an increase of 36% compared to the EC system (11.8 μM). However ·OH radicals are hardly produced in the pure US process, which is only 1.3 μM at 2 h. In order to deeply understand how US improves the generation of ·OH, the electrochemical oxidation channels leading to ·OH formation on the BDD electrode was investigated by DFT calculations. These results are presented later.

Electrochemical properties of BPA with a BDD anode in EC and US–EC processes can be also explored by using potentiostatic i–t curves, as shown in Figure 3. The potentiostatic i–t curves in the stirred solution are recorded with and without 50 mg L^{-1} BPA solution at pH 0 and pH 7 at several applied potentials. In acidic conditions (pH 0) and low applied potential ($E=1.5$ V vs SCE), the steady-state current density in the BPA solution for the US–EC system is 5.39 μA cm^{-2}, higher than for the EC process (1.72 μA cm^{-2}). In solution without BPA the current density also increases from 0.28 to 3.53 μA cm^{-2} with US irradiation. Upon increasing the work potential to 3 V, a similar tendency is obtained, namely that the current density is increased with US in both solutions. In addition, the current density at 3.0 V is much higher (around three orders of magnitude)

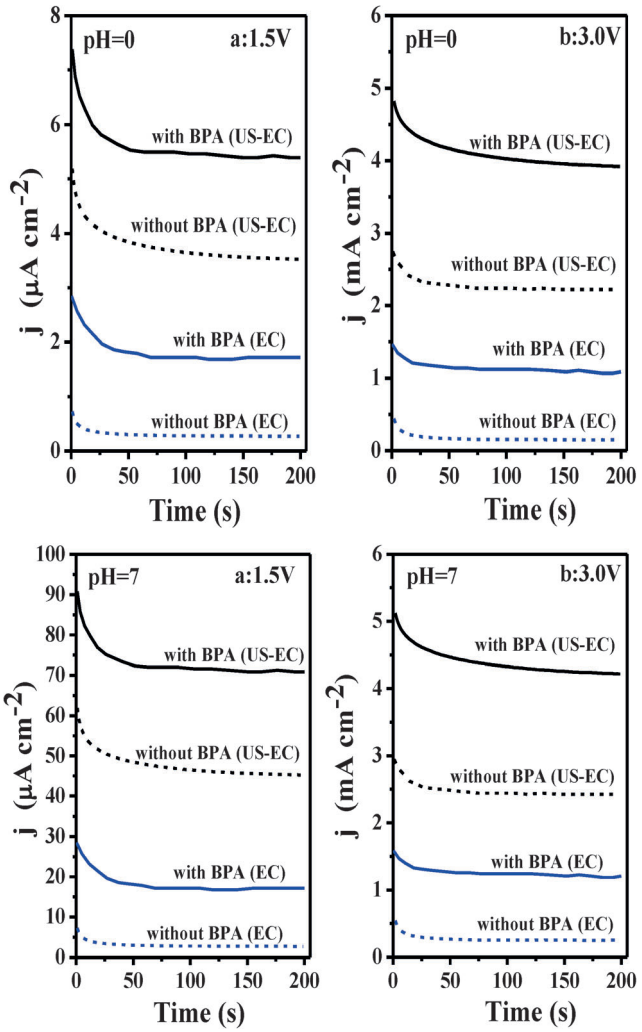

Figure 3. Potentiostatic *I–t* curves at applied potentials (1.5 and 3.0 V) in a 50 mg L^{-1} BPA solution and without BPA solution.

than at 1.5 V for both the EC and the US–EC systems. These results reveal that the current density is quite relevant to the work potential. According to the literature, direct electron transfer reaction would happen in the potential region of water stability ($E < 2.1$ V vs SCE), while indirect oxidation reaction can take place in the potential region of water decomposition ($E > 2.1$ V vs SCE).[9] Moreover, the influence of pH value on the current density of different system was also investigated. At a low potential of 1.5 V, the current density increases with increasing pH value, while it is independent of the pH value at a high potential of 3 V. This result implies that the pH value would influence the surface reaction on BDD at relative low work potentials, which we further investigated by DFT calculations, presented next.

In order to provide deeper insight into the reaction mechanism on BDD surface, for example, to identify the key oxidative intermediate species, we then utilized the recently developed periodic continuum solvation model based on the modified Poisson–Boltzmann equation (CM-MPB) in combination with DFT calculations (DFT/CM-MPB) to model the water oxidation process on the BDD surface at the working potentials. In our calculations, the BDD surface is modeled by a (111) surface with the 1/24 surface C atom being replaced by B. The computational details are shown in the Experimental Section and also in our previous work.[10] To understand the atomic-level mechanism of the reactions on the BDD electrode surface, it is essential to first know the surface composition of BDD, which can be determined by constructing the surface phase diagram from theory.[7,11] Previous work by Chaplin et al.[12] using a cluster model already shows that the surface sites of BDD can be covered by O and OH functional groups at the reaction conditions.

Using the DFT/CM-MPB method, we explored several likely compositions of the BDD surface, that is, 0.5 ML H, 0.13 ML OH, 0.50 ML OH and 0.38 ML OH coadsorbed with 0.13 ML O. The surface phase diagram of BDD was obtained from the computed energetics and is plotted in Figure 4. With an increase in the potential, the surface composition of BDD surface can be described as follows.

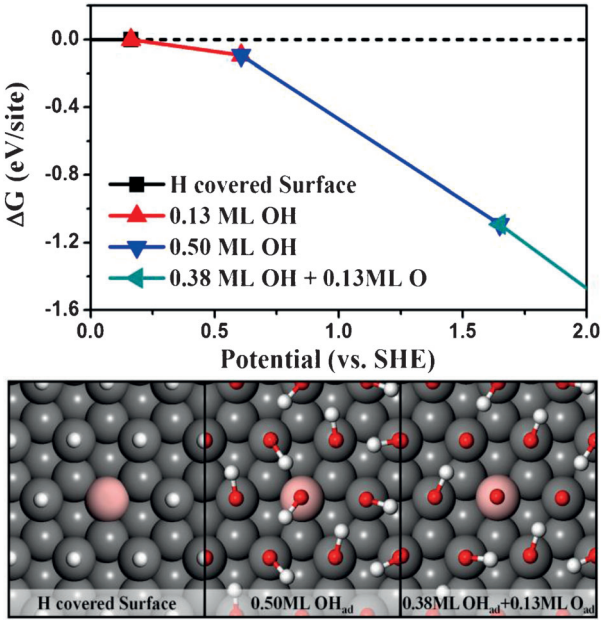

Figure 4. The surface phase diagram of BDD(111) surface under electrochemical conditions (pH 0). The key surface structures are illustrated. Large grey ball: C atoms; large pink ball: B atoms; small write call: H atoms; small red ball: O atoms.

Below 0.25 V, the BDD surface is fully covered (~0.5 ML) by H atoms (dissociated from water) due to the unsaturated nature of the exposed sp^3 carbon atoms. By elevating the potential, the surface H atoms are gradually replaced by atop site adsorbed OH and O. At 0.6 ~1.7 V, a high OH coverage (0.5 ML) on the BDD surface is reached with the surface B atoms and all unsaturated carbon atoms being covered by OH. Above 1.7 V, the adsorbed OH starts to be replaced by the adsorbed O atoms. At that potential, the most stable surface configuration of BDD is a mixed phase, that is, 0.38 ML OH coadsorbed with 0.13 ML O atoms on the BDD surface, denoted as

the OH/O/Sur phase. The adsorbed O atoms (0.13 ML) are neighboring with each other and one O atom adsorbs on the surface B atom (see Figure 4). Further increasing the potential, we expect that the O coverage will increase, but since the oxidation of BPA also starts, it is necessary to consider kinetics to resolve the surface composition.

Because the experimental concerned potential is generally above 1.7 V, where the OH/O/Sur phase dominates, we then select this surface phase as the starting configuration, the initial state (IS), for investigating the water oxidation channels on the BDD surface. The lowest-energy reaction channel at 1.7 V and pH 0 has been determined, as shown in Figure 5. In the first step, the adsorbed O (denoted as *O) on BDD surface react with a nearby H_2O to form an adsorbed OOH (denoted as *OOH) and a solvated proton (H_3O^+) in solution ($*O + 2H_2O_{aq} \rightarrow *OOH + H_3O^+_{aq} + e^-$). At the transition state (TS1 in Figure 5), the O atom of the H_2O bonds forms a bond with the adsorbed O atom at the top site of surface B on BDD surface while meanwhile one H atom of the H_2O molecule transfers to the nearby water molecule. The calculated free energy barrier (ΔG_a) for the first step is 1.95 eV at 1.7 V and the final state (FS), the *OOH and the solvated proton, is 1.32 eV less stable than the IS. Next, the adsorbed OOH undergoes O–OH bond breaking ($*OOH \rightarrow *O + \cdot OH_{aq}$) and at the TS (TS2), the dissociating O–O distance is 1.88 Å with the O atom sitting on the atop sites of surface B and the ·OH stabilized by the water molecule in solution. The ΔG_a of O–OH* dissociation is only 0.46 eV, which is much lower than the first step. Finally, the OH/O/Sur phase of the BDD surface is restored. From Figure 5, we can see that the TS of *OOH formation dictates the highest-energy position in the free energy profile and thus the *OOH formation step should be the rate-determining step. This can be largely attributed to thermodynamics as the *OOH is very unstable on BDD surface at 1.7 V. Based on these results, we can conclude that the atomic adsorbed O atoms are the only likely oxidative species on BDD at low potentials, instead of the adsorbed OOH or solution OH radical.

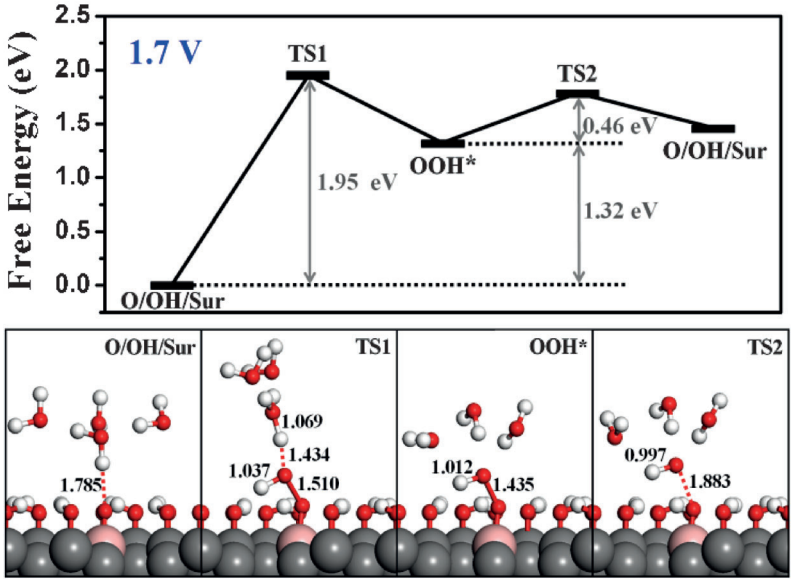

Figure 5. Free energy profile for water oxidation (forming OH radical) on BDD at 1.7 V and pH 0, and the structural snapshots of OH/O/Sur, OOH, TS1 (water dissociation and OOH formation) and TS2 (O–OH dissociation).

To further understand the potential dependence of the reaction profile, we calculated the water oxidation reactions under different surface-charge conditions (charged slab) using the CM-MPB[13] approach. As described in our previous work,[10a,14] the one-to-one mapping of ΔG_a from the constant-charge calculation to the constant potential condition is then performed and thus the reaction profile at the high potentials can be deduced. In Figure 6, we show the reaction profile at 3.0 V and pH 0. We found that at these high potentials ΔG_a for the *OOH formation step is very low, at only 0.09 eV. This is probably because the *OOH formation step involves explicit one-electron transfer ($*O + 2H_2O_{aq} \rightarrow *OOH + H_3O^+_{aq} + e^-$) and the increase in the potential facilitates this reaction. The FS (*OOH and solvated proton) is already 0.16 eV lower than the O/OH/Sur phase. For the next OOH dissociation, we found that the ΔG_a for the O–OH dissociation is 0.63 eV (Figure 6), which is slightly higher than that at 1.7 V. The TS of the O–OH bond breaking (TS2) dictates the highest-energy position in the free energy profile and thus the O–OH bond-breaking step should be rate-determining at high potentials.

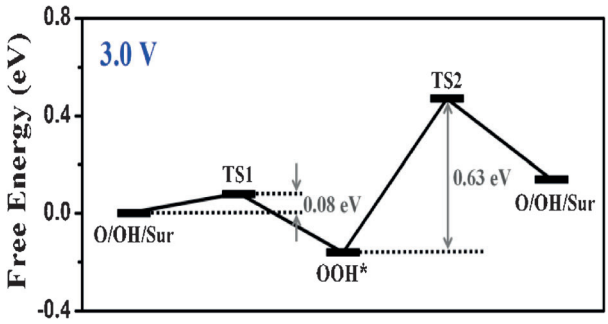

Figure 6. Free energy profile for water oxidation (forming OH radical) on BDD at 3.0 V and pH 0.

Overall, the reaction barrier for the formation of ·OH is only 0.63 eV at 3.0 V, which is 1.32 eV lower than it at 1.7 V. From microkinetics, we expect that the ·OH in solution can be produced at ambient conditions, which can act as the major oxidant to degrade the organic pollutants.

The DFT calculations described above suggest that at low potentials organic pollutants can be degraded by the solution

molecules reacting directly with surface O species, while at high potentials the organic pollutants could also be degraded directly by the ·OH radicals in solution. This is consistent with the experimental observation that the current density at 1.5 V is much lower than that at 3.0 V, considering that the oxidative ability of the adsorbed *O on than BDD surface should be much weaker than that of the ·OH radical. In both cases, the ultrasound can improve the electrochemical oxidation efficiency by enhancing the diffusion and mass transfer of organic pollutants and the ·OH radicals. Furthermore, different oxidants at different potentials from theoretical results can also explain the distinct effects of the pH for the reaction at 1.5 V and 3.0 V (see Figure 3). At low potentials, the surface O coverage can be affected by the concentration of H^+ through the fast reaction equilibrium of $*OH + H_2O \rightarrow *O + H_3O^+ + e^-$. The high pH is beneficial for increasing the O coverage on the BDD surface. By contrast, at high potentials, the O–OH dissociation is essential for increasing the OH radical concentration, which is however not relevant to the pH and thus the influence of the reaction pH can be ignored.

In order to further understand the activation effect of ultrasound in the electrochemical oxidation reaction, a study on the intermediates and their oxidation routes was carried out. The major intermediates, determined by HPLC, are aromatic compounds and chain carboxylic acids, including hydroquinone (HQ), fumaric acid (FA) and oxalic acid (OA) in both EC and US–EC processes (see Figures 7 A–C). According to the literature,[6a,15] the oxidation of BPA by ·OH first leads to phenolic compounds and then can be oxidized and converted to ring-cleavage small fragmented products which would eventually give short-chain aliphatic acids. Additionally, the evolved concentrations of the intermediates obtained were further simulated with a genetic algorithm to determine the formation rate constant (k_f) and the decay rate constant (k_d) of the overall reaction (see Table 1). In the EC process, the intermediates are continuously accumulated at the first stage during anodic oxidation, reaching the maximum concentrations measured in the experiment (C_{max}) and then decreasing at a later stage. For example, the C_{max} of HQ during the EC process is increased to 19.36 mg L^{-1} of 2.0 h, while during US–EC it quickly accumulates, with a C_{max} of 16.24 mg L^{-1} of 1.5 h (Figure 7 A). Moreover, the k_f of HQ is 3.11×10^{-4} s^{-1} in US–EC, 2.2 times greater than that in the EC process (1.41×10^{-4} s^{-1}). The k_d of HQ also increases to 2.23×10^{-4} s^{-1} during the US–EC process from 0.96×10^{-4} s^{-1} during the EC process. The standard errors for k_f and k_d are less than 2%. These results corroborate that aromatics in US–EC process are accumulated more quickly to reach the experimentally measured maximum (C_{max}) and then decrease faster too.

Table 1. Formation rate constant (k_f) and decay rate constant (k_d) of intermediates, maximum concentration and time of intermediates during the degradation in US–EC and EC processes.

Degradation products	$k_f \times 10^4$ [s^{-1}]		$k_d \times 10^4$ [s^{-1}]		C_{max} [mg L^{-1}]		t_{max} [h]	
	US–EC	EC	US–EC	EC	US–EC	EC	US–EC	EC
BPA	–	–	2.4	1.0	50	50	0	0
HQ	3.1	1.4	2.2	1.0	16.2	19.4	1.5	2.0
FA	3.6	27	2.9	2.0	5.3	5.6	1.67	2.5
OA	2.3	1.3	1.8	1.1	13.7	15.6	2.0	3.0

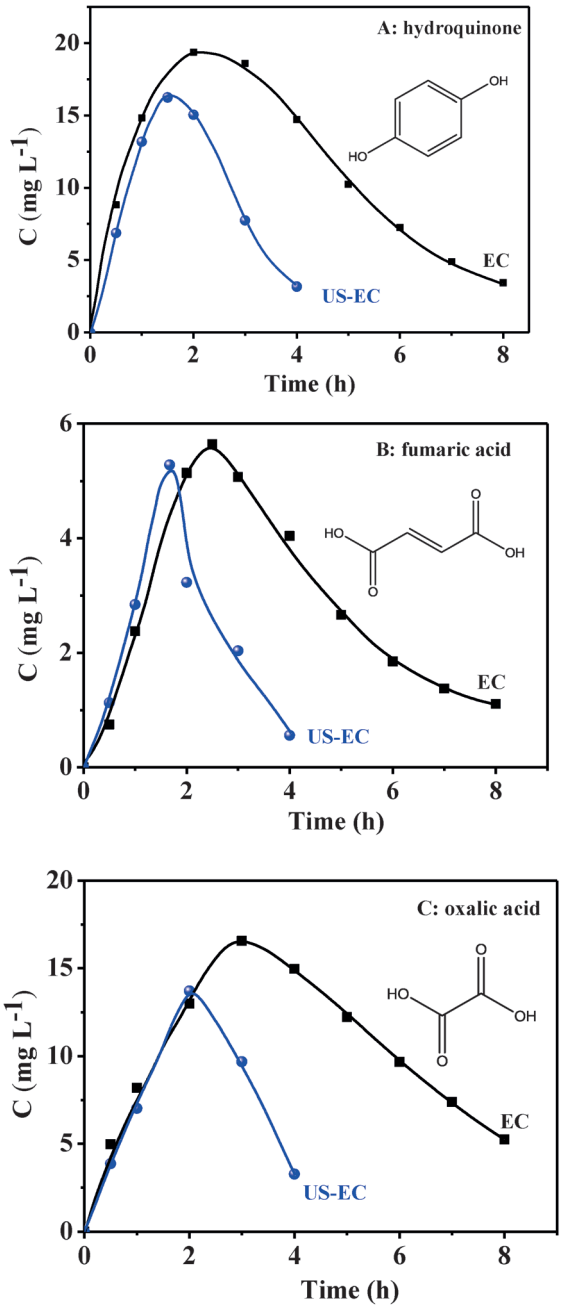

Figure 7. Evolution of the concentrations of aromatic intermediates (A) and carboxylic acid intermediates (B) and (C) during degradation of a 50 mg L^{-1} BPA solution.

The evolution of carboxylic acid, formed from the aromatic cleavage, is depicted in Figures 7 B,C. For the US–EC process, the C_{max} of FA reaches 5.28 mg L^{-1} in 1.67 h and then rapidly oxidizes to OA. The C_{max} of generated OA is 13.71 mg L^{-1} in 1.5 h. During the EC process, the C_{max} of FA is 5.64 mg L^{-1} after

2.5 h anodic oxidation reaction, and the C_{max} of OA is continuously accumulated to 16.56 mg L^{-1} in 3.0 h. In addition, the k_f and k_d of FA for the US–EC process respectively is 3.61×10^{-4} s^{-1} and 2.89×10^{-4} s^{-1}, while for the EC system the k_f and k_d values are 2.67×10^{-4} s^{-1} and 1.98×10^{-4} s^{-1}, respectively. These results show that the k_f and k_d of FA is 1.4 and 1.5 times faster with US–EC comparing to the EC-only process. Similarly the k_f and k_d of OA correspondingly increase 1.8 and 1.7 times respectively for the US–EC process.

As expected, although the rates of formation and degradation are different for the EC and the US–EC processes, the electrochemical oxidation pathway of BPA with BDD electrode does not change with the assistance of US. That is to say US mainly improve the diffusion and mass transfer of organic pollutants and/or oxidative radicals, which is consistent with the DFT calculation analysis and the potentiostatic *i–t* results.

3. Conclusions

This study reported the reaction activity and pathway for removing BPA in EC and US–EC processes with a BDD electrode. The degradation efficiency was improved with the aid of US, which was evaluated by BPA removal and COD removal. The structure and stability of the BDD surface was illustrated by DFT calculations, and the reaction channel for the potential-dependent kinetics of hydroxyl radical (·OH) generation was also investigated by means of DFT.

The BPA removal increased from 79% for the EC process to 98% for the US–EC process after 4 h electrolysis, while the removal of COD improved from 73% for EC to 94% for US–EC. A study of the kinetics indicates that BPA decay follows a pseudo-first-order reaction, with a higher rate constant for the US–EC process. The most stable surface configuration of BDD is relevant to the work potential. At 1.7 V, the stable BDD surface consisted of 0.38 ML OH coadsorbed with 0.13 ML O atoms. With increasing work potential, the O coverage increased and was eventually replaced by O species, such as OOH and molecular O_2. During the EC reaction, at low work potential (i.e.,1.7 V), the reaction activity was mainly influenced by direct electrolysis and the only likely oxidative species on the BDD surface was atomic adsorbed *O atoms, while at high potential (i.e., 3 V), the formed free ·OH in solution after O–OH dissociation became the major oxidant to degrade organic pollutants. Thus, in the enhanced US–EC process, ultrasound increased the diffusion and mass transfer of ·OH at high working potential, while enhancing the collision frequency between organic pollutants and O* radical, alleviating electrode fouling at a low working potential.

Furthermore, aromatic and carboxylic intermediates of BPA were identified and quantified by HPLC. The primary intermediates both in US–EC and EC processes include HQ, FA and OA, indicating the same degradation pathway of BPA. The values k_f and k_d of the intermediates are enhanced in the US–EC process. The experimental results again confirmed the observation of DFT calculation that US mainly enhanced diffusion and mass transfer of mediated oxidants.

Experimental Section

Reagents and Apparatus

BPA was from Sigma and all reagents were of analytical grade. HQ, OA, FA, dimethyl sulfoxide, 2,4-dinitrophenylhydrazine, organic solvents and other chemicals used were analytical grade. All solutions were prepared with deionized water. EC measurements were carried out on a CHI 660 electrochemical work station (CHI Co., USA). The ultrasonic generator was a CQ/50 ultrasonic instrument (Shanghai Ultrasonic Instrument Co., China).

Electrochemical Degradation

Electrochemical measurements were carried out in a conventional three-electrode cell using a CHI 660 electrochemical workstation (CHI Co., USA). A BDD electrode was used as the working electrode, with saturated calomel electrode (SCE) as a reference, and Pt as a counter electrode. The concentration of BPA in solution with 0.05 M Na_2SO_4 was 50 mg L^{-1}. All potentials in this work were against SCE.

EC oxidation of BPA was carried out in a cylindrical single-compartment cell with a jacketed cooler to maintain a constant temperature of 20 °C. The BDD electrode worked as anode with an immersed area of 3 cm^2. BDD thin films were deposited on a *p*-Si(100) surface (area 15 mm × 15 mm) which had been pretreated by polishing with hydrogen for 20 min at low pressure by a wave-assisted chemical vapor deposition (MP-CVD) system. The crystallites in these polycrystalline films were of high structural quality, and the size ranged from 5 to 10 μm. The thickness of the obtained diamond film was about 1 μm. A titanium foil with the same area was used as cathode and the electrode gap was 1 cm. The solution was electrolyzed at a constant current density of 20 mA cm^{-2}. The BPA solution of 50 mg L^{-1} was degraded in an aqueous medium containing 0.05 M Na_2SO_4 as supporting electrolyte. US–EC degradation was carried out at a frequency of 33 kHz, with a delivered power of 50 W, and other conditions were the same as those in the EC process.

Analysis

The evolution of BPA and its intermediates were measured by HPLC (Agilent HP 1100, Agilent, USA) system. Chromatographic separations were performed on an analytical column Ultimat TMAQ-C18 (5 μm, 4.6 × 100 mm), with the column at room temperature and selected UV detector at $\lambda = 230$ nm. For these analyses, a 60:40 (v/v) methanol/buffer (pH 2.3) of 1:2 (v/v) 50 mmol NaH_2PO_4/50 mmol H_3PO_4 was employed according to the mobile phase at a flow rate of 1.0 mL min^{-1}. 20 μL aliquots were injected into the HPLC chromatograph.

Assuming that the formation and decay of each intermediate were pseudo-first-order reactions, the formation reaction rate constant k_f and decay reaction rate constant k_d are calculated according to Equation (1):[16]

$$C_B = C_0 \frac{k_f}{k_d - k_f}\left(e^{-k_f t} - e^{-k_d t}\right) \quad (1)$$

where C_B is the intermediates concentration, C_0 is the BPA initial concentration. A genetic algorithm, as a promising stochastic optimization method, was used to fit the data, determining k_f and k_d. The hydroxyl radicals were determined according to literature,[17] in which formaldehyde was generated quantitatively by the reaction

between hydroxyl radicals and dimethyl sulfoxide (DMSO). Then the formaldehyde reacted with 2,4-dinitrophenylhydrazine (DNPH) to form the corresponding hydrazone (HCHO–DNPH), which was analyzed by HPLC (Agilent HP 1100, Agilent, USA). An Agilent Zorbax Eclipse XDB-C18 column (150×4.6 mm, particle size 5 μm) was used at room temperature and with selected UV detector at $\lambda = 355$ nm. To perform the isocratic elution at a flow rate of 1.0 mL min^{-1}, a mixture of methanol and water (60:40, v/v) was used as mobile phase. The chemical oxygen demand (COD) was determined by the standard colorimetric (titrimetric) method with closed reflux.

DFT Calculations

All density functional theory (DFT) calculations were performed using the SIESTA package[18] with numerical atomic orbital basis sets[19] and Troullier–Martins norm-conserving pesudopotentials.[20] The exchange–correlation functional utilized was at the generalized gradient approximation level, known as GGA-PBE.[21] The optimized double-ζ plus (DZP) polarization basis set with extra diffuse functions was employed. The orbital-confining cutoff was determined from an energy shift of 0.010 eV. The energy cutoff for the real space grid used to represent the density was set as 150 Ry. Monkhorst–Pack of *k*-point sampling with a (2×2×1) mesh was used in all calculations. A larger energy cut-off of 250 Ry and the denser (4×4×1) *k*-point mesh were used later for converging the energetics of the water oxidation reactions. The quasi-Newton–Broyden method was employed for geometry relaxation until the maximal forces on each relaxed atom were less than 0.05 eV Å^{-1}. Spin-polarization was considered in all calculations. To correct the zero-point energy (ZPE), vibrational frequency calculations were performed via the finite-difference approach. The transition states (TSs) of the catalytic reaction were searched by using the constrained-Broyden–dimer method.[22]

For the calculation of the surface adsorption structures and water oxidation energy profile, we utilized ($3\times2\sqrt{3}$) (24 atoms per layer) six-layer symmetrical slabs with adsorbates on both sides of the (111) surfaces. In our modelling, the reaction occurs on both sides of the surfaces, which is essential for an accurate measurement of the electrochemical potential of the system. Because the B atom prefers three-fold coordination, the structure model of BDD is a 1/24 ML B-doped BDD(111) surface, that is, a surface C atom (three-coordinated) being replaced by a B atom per unit cell (the exact model for BDD is not known from experiment). The middle two layers in the six-layer slab were held at the bulk truncated position of diamond and the other layers were fully relaxed in calculations.

To derive the free energy reaction profile, we first obtain the reaction energy of each step (strictly speaking, the Helmholtz free energy change (ΔF) at 0 K, 0 bar) that is directly available from the DFT total energy (ΔE) after the ZPE correction. For elementary surface reactions without involving the adsorption/desorption of gaseous or liquid molecules, ΔF at 0 K, 0 bar is a good approximation to the Gibbs free energy (ΔG) as the temperature T and pressure p contributions at the solid phase are small. To compute the free energy change ΔG of elementary reactions involving gaseous or liquid molecules, such as oxygen, hydrogen, and water, the large entropy term at 298 K is essential to take into account. We utilize the standard thermodynamic data[23] to obtain the temperature and pressure contributions for the G of the aqueous H_2O and gaseous H_2, which are −0.57 eV (the entropy contribution is −0.22 eV in solution) and −0.31 eV compared to the total energy of the corresponding free molecule (E, 0 K), respectively.[24] The G of O_2 is derived as $G[O_2] = 4.92\ [eV] + 2G[H_2O] - 2G[H_2]$ by utilizing the OER equilibrium at the standard conditions.

DFT-Based Modified Poisson–Boltzmann Approach for Electrochemistry

Our methodology for calculating electrocatalytic reactions has been described in recent publications.[10] The solid–liquid interface was described using the periodic continuum solvation model based on the modified Poisson–Boltzmann equation (CM-MPB), which can take into account the long-range electrostatic interaction due to the solvation of electrolyte.[13] The DFT/CM-MPB method has been utilized to calculate the electrocatalytic oxygen reduction reactions at solid–liquid interfaces,[10] and to compute the fundamental properties of metal surfaces in solution, such as the potential of zero charge and the differential capacitance, where the calculated values show good agreement with the available experimental data.[13]

For modeling reactions involving ions, both the implicit (CM-MPB) and the explicit (H_2O molecules) solvation need to be taken into account due to the strong polarization of the ionic species in solution. For example, for proton, H_3O^+, we must also include its first solvation shell to model the reacting proton in solution, that is, $H_3O^+(H_2O)_3$ in bulk solution and $H_3O^+(H_2O)_2$ at the solid–liquid interface (the rest of the solution is represented by the CM-MPB model). At the solid–liquid interface, two of the H atoms of H_3O^+ are hydrogen-bonded with the nearby water molecules, and the remaining H can interact with the surface electronegative species such as O_2, O, and OH. The explicit solvation has also been checked for other reactions by adding extra H_2O molecules near the reactants.

Acknowledgements

This work was supported jointly by the National Natural Science Foundation P.R. China (Project No. 21277099, 21207101, 21173051, 21361130019), 973 program (2011CB808500, 2013CB834603), Science and Technology Commission of Shanghai Municipality (08DZ2270500), Program for Professor of Special Appointment (Eastern Scholar) at the Shanghai Institute of Higher Learning, a China Postdoctoral Science Foundation funded project (2013M531112), Shanghai Postdoctoral Scientific Program (13R21410300) and supported by the Fundamental Research Funds for the Central Universities.

Keywords: boron-doped diamond electrodes · bisphenol A · density functional calculations · electrochemical oxidation · ultrasound

[1] a) X. W. He, Z. Chai, F. P. Li, C. H. Zhang, D. Li, J. Li, J. L. Hu, *J. Chem. Technol. Biotechnol.* **2013**, *88*, 1568–1575; b) B. H. Wang, H. J. Wu, G. X. Zhang, S. Licht, *ChemSusChem* **2012**, *5*, 2000–2010.
[2] M. Panizza, G. Cerisola, *Chem. Rev.* **2009**, *109*, 6541–6569.
[3] I. Sirés, E. Brillas, M. A. Oturan, M. A. Rodrigo, M. Panizza, *Environ. Sci. Pollut. Res. Int.* **2014**, *21*, 8336–8367.
[4] X. P. Zhu, J. R. Ni, P. Lai, *Water Res.* **2009**, *43*, 4347–4355.
[5] a) S. Saiyood, A. S. Vangnai, P. Thiravetyan, D. Inthorn, *J. Hazard. Mater.* **2010**, *178*, 777–785; b) C. A. Staples, P. B. Dorn, G. M. Klecka, S. T. O'Block, L. R. Harris, *Chemosphere* **1998**, *36*, 2149–2173.
[6] a) Z. B. Guo, R. Feng, *J. Hazard. Mater.* **2009**, *163*, 855–860; b) Y. H. Cui, X. Y. Li, G. H. Chen, *Water Res.* **2009**, *43*, 1968–1976; c) A. O. Kondrakov,

A. N. Ignatev, F. H. Frimmel, S. Brase, H. Horn, A. I. Revelsky, *Appl. Catal. B* **2014**, *160*, 106 – 114.
[7] a) J. Rossmeisl, G. S. Karlberg, T. Jaramillo, J. K. Nørskov, *Faraday Discuss.* **2008**, *140*, 337 – 346; b) H. A. Hansen, J. Rossmeisl, J. K. Norskov, *Phys. Chem. Chem. Phys.* **2008**, *10*, 3722 – 3730.
[8] a) X. M. Chen, G. H. Chen, F. R. Gao, P. L. Yue, *Environ. Sci. Technol.* **2003**, *37*, 5021 – 5026; b) J. Jeong, J. Y. Kim, J. Yoon, *Environ. Sci. Technol.* **2006**, *40*, 6117 – 6122.
[9] J. Iniesta, P. A. Michaud, M. Panizza, G. Cerisola, A. Aldaz, C. Comninellis, *Electrochim. Acta* **2001**, *46*, 3573 – 3578.
[10] a) G. F. Wei, Y. H. Fang, Z. P. Liu, *J. Phys. Chem. C* **2012**, *116*, 12696 – 12705; b) G. F. Wei, Z. P. Liu, *Phys. Chem. Chem. Phys.* **2013**, *15*, 18555 – 18561.
[11] G. F. Wei, Z. P. Liu, *Energy Environ. Sci.* **2011**, *4*, 1268 – 1272.
[12] B. P. Chaplin, D. K. Hubler, J. Farrell, *Electrochim. Acta* **2013**, *89*, 122 – 131.
[13] Y. H. Fang, G. F. Wei, Z. P. Liu, *Catal. Today* **2013**, *202*, 98 – 104.
[14] Y. H. Fang, G. F. Wei, Z. P. Liu, *J. Phys. Chem. C* **2014**, *118*, 3629 – 3635.
[15] M. Murugananthan, S. Yoshihara, T. Rakuma, T. Shirakashi, *J. Hazard. Mater.* **2008**, *154*, 213 – 220.
[16] a) M. H. Fatemi, *Anal. Chim. Acta* **2006**, *556*, 355 – 363; b) J. X. Gao, G. H. Zhao, W. Shi, D. M. Li, *Chemosphere* **2009**, *75*, 519 – 525; c) L. Liu, G. H. Zhao, M. F. Wu, Y. Z. Lei, R. Geng, *J. Hazard. Mater.* **2009**, *168*, 179 – 186.
[17] C. Tai, J. F. Peng, J. F. Liu, G. B. Jiang, H. Zou, *Anal. Chim. Acta* **2004**, *527*, 73 – 80.
[18] J. M. Soler, E. Artacho, J. D. Gale, A. Garcia, J. Junquera, P. Ordejon, D. Sanchez-Portal, *J. Phys. Condens. Matter* **2002**, *14*, 2745 – 2779.
[19] J. Junquera, O. Paz, D. Sanchez-Portal, E. Artacho, *Phys. Rev. B* **2001**, *64*, 235111.
[20] N. Troullier, J. L. Martins, *Phys. Rev. B* **1991**, *43*, 1993 – 2006.
[21] J. P. Perdew, K. Burke, M. Ernzerhof, *Phys. Rev. Lett.* **1996**, *77*, 3865 – 3868.
[22] C. Shang, Z. P. Liu, *J. Chem. Theory Comput.* **2010**, *6*, 1136 – 1144.
[23] *CRC Handbook of Chemistry and Physics, 84th ed.*, CRC press, **2003 – 2004**.
[24] Z. P. Liu, S. J. Jenkins, D. A. King, *J. Am. Chem. Soc.* **2004**, *126*, 10746 – 10756.

Received: November 4, 2014
Published online on December 17, 2014